Journal of Membrane Science 661 (2022) 120944

Contents lists available at ScienceDirect

Journal of Membrane Science

journal homepage: www.elsevier.com/locate/memsci

Boosting the permeation of ultrafiltration membranes by covalent organic frameworks nanofillers: Nanofibers doing better than nanoparticles

Guanghui Yang, Zhe Zhang **, Congcong Yin, Xiansong Shi, Yong Wang *

State Key Laboratory of Materials-Oriented Chemical Engineering, and College of Chemical Engineering, Nanjing Tech University, Nanjing, 211816, Jiangsu, PR China

ARTICLE INFO

Keywords:
Covalent organic frameworks (COFs)
Nanofibers
Nanoparticles
Mixed matrix membranes (MMMs)
Ultrafiltration

ABSTRACT

Mixed matrix membranes (MMMs) have attracted everlasting attentions, as their large permeance and high selectivity can be accessible synchronously. Herein, we show that covalent organic framework (COF) nanofibers serving as the nanofillers are doing better than COF nanoparticles in boosting the separation performance of MMMs. The nanofibers and the nanoparticles are synthesized and doped into polysulfone matrices to prepare MMMs. The high porosity and relative hydrophilicity of TpPa nanofibers and nanoparticles enable rapid exchange of solvent and nonsolvent during the process of nonsolvent induced phase separation, thus leading to instantaneous demixing. Furthermore, compared with TpPa nanoparticles possessing small and irregular shapes, the one-dimensional structure of TpPa nanofibers weakens the entanglement of the surrounding polysulfone linear chains, resulting in much pronounced instantaneous demixing. In contrast with the nanoparticle-incorporated membranes, the porosity of nanofiber-incorporated membranes is significantly improved. The resultant nanofiber-incorporated membrane demonstrates a high water permeance of 424.4 L m^{-2} h^{-1} bar^{-1}, along with a BSA rejection rate of 94.3%. This work clearly reveals that porous one-dimensional structures such as COF nanofibers are highly promising in the preparation of high-performance MMMs.

1. Introduction

Ultrafiltration is a pressure-driven membrane separation technique that has received considerable attention for its excellent efficacy and applicability in selectively removing viruses, natural organic matters, and colloidal particles from water [1,2]. Membrane materials are the cornerstone for the membrane separation process, as they largely dominate the microstructures and the functionalities of the membranes. This would further influence the separation performance of the membranes. Nonsolvent-induced phase separation (NIPS) is a typical method for fabricating ultrafiltration membranes. It produces an asymmetric and integral membrane, which consists of a nanoporous skin layer as well as a macroporous support layer [3,4]. To date, a wide array of polymers including polysulfone (PSF) [5,6], polyether sulfone (PES) [7,8] and polyvinylidene fluoride (PVDF) [9,10], have been adopted as the membrane materials. Those membranes have showcased favourable separation performances. However, given the inherent hydrophobicity of those polymers [11,12], the membranes inevitably suffer from poor surface hydrophilicities and unsatisfied porosities. This further results in sluggish water permeation, or even worse, deteriorated selectivity. Therefore, enhancing the water permeance without compromising the selectivity is of paramount significance to meet the demand of efficient ultrafiltration. Yet, it still poses a major issue.

Doping nanofillers into polymer matrices to prepare mixed matrix membranes (MMMs) is effective for enhancing the water permeance [13–15]. It is widely proved that the nanofillers can influence the thermodynamics and the kinetics of polymer solutions during the NIPS process. Thus, orchestrating those parameters would be beneficial to optimize the microstructures and surface properties of the membranes, such as the porosities and the surface hydrophilicities. Especially, the improved porosities create a large number of nanopores, which can be used as additional channels for water permeation [16–18]. As a result, the water permeance would be greatly enhanced. However, the most commonly used nanofillers including inorganic nanofillers and inorganic-organic hybrid nanofillers do not possess a favourable affinity toward the polymer matrices. In light of the inadequate compatibility between the nanofillers and the matrices, interfacial defects would be inevitably formed, ultimately deteriorating the selectivity to some

* Corresponding author.
** Corresponding author.
E-mail addresses: zhangzhe@njtech.edu.cn (Z. Zhang), yongwang@njtech.edu.cn (Y. Wang).

https://doi.org/10.1016/j.memsci.2022.120944
Received 19 July 2022; Received in revised form 9 August 2022; Accepted 18 August 2022
Available online 22 August 2022

extent. Therefore, should the nanofillers with better compatibility be used, the highly efficient ultrafiltration process of the MMMs could be realized.

Covalent organic frameworks (COFs) are a type of porous and crystalline framework materials which are formed by the reticulation process. The building blocks are interlinked through the covalent bonds so as to form extended structures with long-range order [19–21]. COFs possess various superiorities including well-defined nanopores, good thermal/chemical stabilities, high surface areas and readily-custom functionalities [22–24]. In particular, the large porosity, good stabilities as well as the wholly organic backbones make COFs highly promising in the fabrication of MMMs [25]. The organic nature of COFs offers the high affinity toward the polymer matrices that improves the compatibility between the nanofillers and the matrices substantially. Additionally, the good stability against water ensures that the COFs can maintain their structural integrality during both the NIPS and the separation processes [26]. A few seminal works have demonstrated that the COFs being either doped or in situ formed in polymer matrices are capable of enhancing the water permeance while maintaining satisfactory rejections [27–29]. In those works, COFs with two-dimensional and three-dimensional structures, that is, the planar sheets and nanoparticles, were used as the nanofillers. Given the one-dimensional structure of COF nanofibers, they would influence the entanglement of the linear polymer chains which have similar one-dimensional structures. It is anticipated to give unique influences on the thermodynamics and the kinetics of the casting solution during the NIPS process. Therefore, the separation performances are expected to be significantly boosted. However, the effects of one-dimensional COFs on the phase separation as well as the separation performance remain unexplored.

Herein, we developed a strategy using one-dimensional COF nanofibers as the nanofillers to prepare ultrafiltration membranes with significantly boosted water permeance. TpPa nanofibers were doped into polysulfone matrix to prepare MMMs via NIPS process. To highlight the advantages of the nanofibers, TpPa nanoparticles were also doped into the matrix to prepare control membrane. TpPa nanofibers and nanoparticles conferred rapid exchange between solvent and nonsolvent during NIPS process, resulting in instantaneous demixing. Moreover, much pronounced instantaneous demixing can be found in the case of TpPa nanofibers being doped, compared with that of TpPa nanoparticles. Therefore, the porosity of the nanofiber-incorporated membranes was significantly improved. The resultant membranes exhibited large water permeance and high BSA rejection rate. This work demonstrated the superiority of TpPa nanofibers in enhancing the performance of ultrafiltration membranes, paving a pathway for the fabrication of high performance MMMs.

2. Experimental

2.1. Materials

1,3,5-Triformylphloroglucinol (Tp) was purchased from Jilin Chinese Academy of Sciences-Yanshen Technology Co., Ltd. Surfactants including sodium dodecyl sulfate (SDS), hexadecyl trimethyl ammonium bromide (CTAB) as well as *p*-phenylenediamine (Pa) were provided by Aladdin. Bovine serum albumin (BSA) as well as phosphate buffered saline (PBS) tablets were provided by MP Biomedicals. Polysulfone pellets (Udel P-3500) were supplied by Solvay. Polyester nonwoven fabrics were supplied by Teijin Limited. Other reagents including 1,4-dioxane, *N*,*N*-dimethylacetamide (DMAc), ammonia water and acetic acid were obtained from local suppliers. All chemical reagents used throughout this work were all in analytical grade. Deionized water was used in this work.

2.2. Synthesis of TpPa

TpPa nanofibers were prepared according to our previous work [30, 31], while TpPa nanoparticles were prepared by a conventional solvothermal method (Experimental details are shown in Supplementary Information).

2.3. Fabrication of membranes

The illustration of the fabrication of MMMs is shown in Scheme 1. The mass fraction of PSF in the casting solution was fixed at 18 wt% (by weight of the casting solution). The mass fraction of TpPa nanofibers in the casting solution were 0.05, 0.1, 0.15 and 0.2 wt%, respectively (by weight of PSF). TpPa nanofibers were first added into DMAc, and ultrasonically treated for 10 min to make them uniformly dispersed. Then, a certain amount of PSF pellets were added into the above solution and mechanically stirred at 70 °C for 6 h. The solution was then allowed to stand undisturbed for 12 h to eliminate air bubbles, and the casting solution for membrane fabrication was obtained.

The membranes were prepared on an automatic film applicator (JFA-II, Shanghai Modern Environment Engineering Technique Co., Ltd.). The nonwoven fabric was placed on the applicator, followed by pouring out the casting solution onto it. Then, the casting solution was spread using a 200-μm-height knife. As-coated nonwoven fabric was immediately immersed in water at room temperature for phase separation. Finally, the obtained membranes were thoroughly washed and stored in water. Note that, PSF membranes incorporated with 0.1 wt% of TpPa nanofibers were used for further tests. For comparison, PSF membranes incorporated with 0.1 wt% of TpPa nanoparticles were fabricated by the same procedure. The pristine PSF membranes were also fabricated by the same procedure except for the addition of TpPa.

2.4. Characterizations

The composition and crystallinity of TpPa were characterized by Fourier transform infrared (FTIR, Nicolet 8700, Thermo Fisher Scientific) spectroscopy and X-ray diffraction (XRD, Smart Lab, Rigaku), respectively. The morphologies of TpPa and membranes were observed by scanning electron microscopy (SEM, S-4800, Hitachi). To enhance the conductivity, samples were sputter-coated with an ultrathin layer of gold. Nitrogen adsorption experiments were conducted on a ASAP2460 porosimetry system (Micromeritics). The pore width distribution was obtained based on the nonlocal density functional theory (NLDFT). The roughness of the membranes was recorded using an atomic force microscopy (AFM, XE-100 system, Park Systems). A Drop Meter A100P goniometer (MAIST) was adopted to measure water contact angles of the membranes surface. A laser scanning spectral confocal microscope (LSCM, Leica TCS SP2, Leica Microsystems) was used to investigate the distribution of TpPa within PSF matrices via fluorescence imaging. The viscosity of the casting solution was measured using a rotational viscometer (DV2T, Brookfield) at room temperature with a speed of 10 rpm. The surface porosity as well as pore size distribution of different membranes were determined from their surface SEM images using the ImageJ software, following the protocol reported in literature [32]. The overall porosity of membrane was measured by the weighing method, which can be described as follows [9,33]:

$$\varepsilon_A = (W_1 - W_2) / (S\, d_m\, \rho_w) \quad (1)$$

where ε_A (%) is the overall porosity of the membrane, W_1 (mg) and W_2 (mg) are the wet weight and dry weight of the membrane, respectively, S (cm^2) is the effective area, d_m (cm) is the membrane thickness, and ρ_w (mg cm^{-3}) is water density.

The cloud point of the casting solution with and without TpPa were conducted by the titration method at room temperature [34,35]. A small amount of water serving as the nonsolvent was slowly added into the homogenous casting solution under a continuous stirring. When water was dropped into the solution, the precipitation in a very local area occurred, and such precipitates would be redissolved under the stirring.

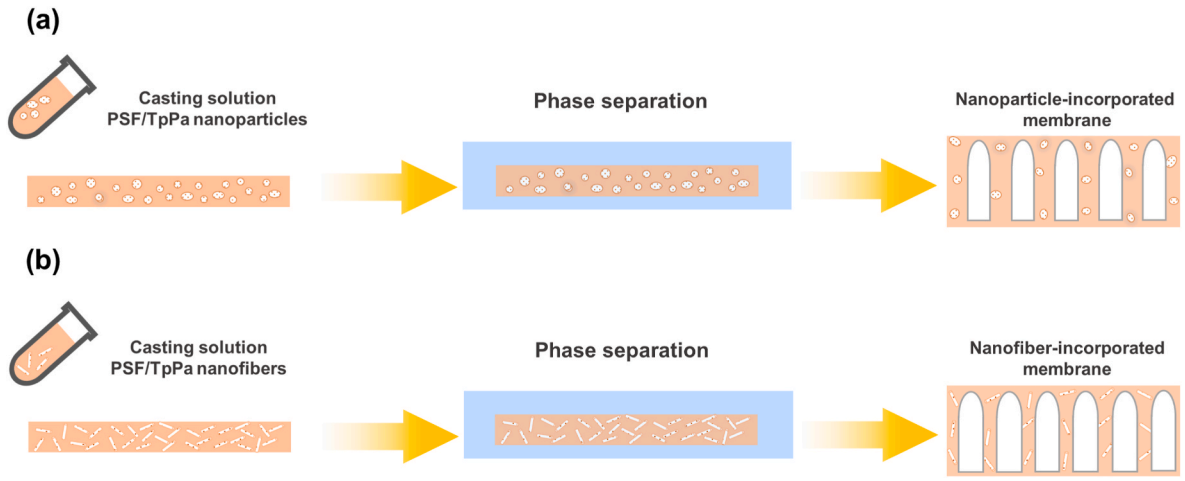

Scheme 1. Illustration of the fabrication of MMMs. (a) The fabrication of the nanoparticle-incorporated membrane. (b) The fabrication of the nanofiber-incorporated membrane.

Once the precipitates could not be redissolved, that is, the solution became turbid. This state can be described as the cloud point, and the dosage of water was recorded accordingly.

2.5. Ultrafiltration performance test

The water permeance and BSA rejection rate of membranes were measured on a cross-flow unit (SF-SB, Hangzhou Saifei Membrane Separation Co., Ltd.). Three test cells were assembled in parallel, and the effective membrane area of each cell was 7.1 cm^2. The transmembrane pressure was maintained at 2 bar, and the flow rate was 30 L h^{-1}. The liquid temperature during the test was 25 °C. Membranes were pre-compacted under a pressure of 2 bar for 30 min. The concentration of BSA aqueous solution (with PBS) was 0.5 g L^{-1}. The concentration of each BSA sample was determined using a Nanodrop 2000c UV–vis spectrophotometer (Thermo Fisher Scientific). The water flux (J_w, L m^{-2} h^{-1}), water permeance (P_w, L m^{-2} h^{-1} bar^{-1}) and BSA rejection rate (R, %) were calculated as below:

$$J_w = \Delta V / (A\ \Delta t) \quad (2)$$

$$P_w = J_w / \Delta p \quad (3)$$

$$R = (1 - C_p / C_f) \times 100\% \quad (4)$$

where ΔV (L) is the volume of the permeated solution, A (m^2) is the effective filtration area of the membrane, Δt (h) is the permeating duration, and Δp (bar) is the transmembrane pressure. C_p and C_f are the BSA concentrations of the permeated solution and the feed, respectively

3. Results and discussion

3.1. Characterization of TpPa

TpPa nanofibers were prepared via a method of surfactant-mediated solvothermal synthesis based on our previous work (Fig. S1a) [30,31]. The one-dimensional and fibrous morphology was confirmed by SEM observation (Figs. S1b and c). The chemical structure of TpPa nanofibers was verified by FT-IR spectrum, as the characteristic peaks of C═C and C–N originating from the β-ketoenamine linkage appeared at 1582 cm^{-1} and 1276 cm^{-1}, respectively (Fig. S1d) [26]. XRD pattern of TpPa nanofibers exhibited a distinct peak at ~4.7°, which corresponds to the (100) crystallographic plane (Fig. S1e) [26]. The surface area of TpPa nanofibers was 383.4 m^2 g^{-1} (Fig. S1f), and the mean pore width was centered at 1.3 nm (Fig. S1g). TpPa nanoparticles used for the comparison were prepared by the conventional solvothermal method (Fig. S2a). TpPa nanoparticles possess three-dimensional and irregularly-shaped morphologies, as large bulks and small flakes can be observed by SEM (Figs. S2b and c). The chemical structure and crystalline structure of TpPa nanoparticles were verified by FT-IR spectrum and XRD pattern, respectively (Figs. S2d and e). The surface area of TpPa nanoparticles was 651.9 m^2 g^{-1} (Fig. S2f), and the mean pore width was centered at 1.6 nm (Fig. S2g). All above results validate that TpPa nanofibers and nanoparticles featuring ordered pore channels, high porosity and favourable crystallinity were synthesized.

3.2. Characterization of membranes

TpPa nanofibers and nanoparticles were doped into PSF matrices to prepare MMMs. Considering that TpPa possesses a fluorescence property, the distribution of TpPa in MMMs was visualized by the fluorescence imaging [36]. As shown in Fig. 1, the pristine PSF membrane did not show any fluorescence. After the incorporation of TpPa nanofibers and nanoparticles, green fluorescence appeared throughout the cross sections of both membranes. This result provides direct evidence for the incorporation of TpPa into PSF matrices. It should be underlined that the strong fluorescence emerged in both membranes, in spite of a small amount of nanofibers and nanoparticles being incorporated. This is indicative of even distribution of nanofibers and nanoparticles within PSF matrices, as result of the low density of TpPa. Note that, the brightness and contrast of images merely relate to the flatness of the cross sections, instead of the distribution of TpPa. In addition, the membranes possessed a similar thickness of ~60 μm.

The morphologies of membranes were then investigated by SEM. The surface and cross-sectional SEM images are shown in Fig. 2. It can be directly seen that the surface and cross-sectional morphologies of membranes were obviously changed, after the incorporation of TpPa nanofibers and nanoparticles. For the surface, much larger pores were found in the nanofiber-incorporated membrane and the nanoparticle-incorporated membrane, compared with that of the PSF membrane. Based the analysis of the pore size distribution, the pore size of PSF membrane, nanofiber-incorporated and nanoparticle-incorporated membranes were 10.5 nm, 16.8 nm and 15.4 nm, respectively (Fig. S3). According to the cross-sectional images, all membranes showed a typical asymmetric structure, consisting of an upper skin layer and a support layer with finger-like pores, regardless of the incorporation of TpPa. The thicknesses of these membranes were nearly the same (~60 μm), which are in line with those in the fluorescence images. The finger-like pores of the nanofiber-incorporated membrane and the nanoparticle-incorporated membrane became larger and elongated,

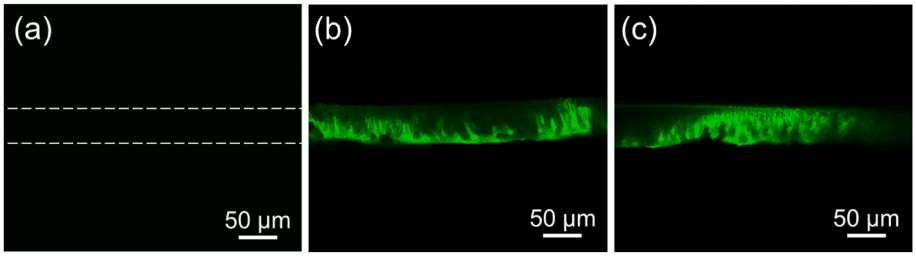

Fig. 1. Fluorescence microscopy images of different membranes. (a) PSF membrane. (b) Nanofiber-incorporated membrane. (c) Nanoparticle-incorporated membrane.

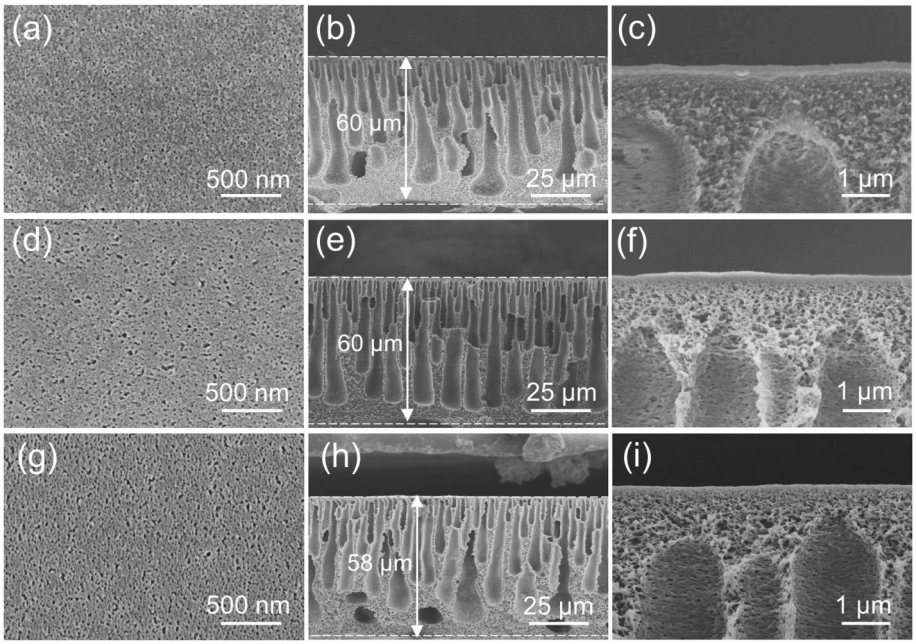

Fig. 2. Morphological characterization by SEM. (a) Surface and (b and c) cross-sectional images of PSF membranes. (d) Surface and (e and f) cross-sectional images of nanofiber-incorporated membranes. (g) Surface and (h and i) cross-sectional images of nanoparticle-incorporated membranes.

after the incorporation of TpPa. Moreover, the finger-like pores of the nanofiber-incorporated membrane are somewhat larger than those of the nanoparticle-incorporated membrane. It should be noticeable that TpPa nanofibers did not appear at both surface and cross section of nanofiber-incorporated membrane. It is mainly because a small amount of TpPa nanofibers with small size were well dispersed in PSF matrices. However, some large bulks of TpPa nanoparticles were found at the cross section of the nanoparticle-incorporated membrane, which is in line with their three-dimensional and irregularly-shaped morphologies (Fig. S4).

To further understand the porosity changes influenced by the incorporation of TpPa nanofibers and nanoparticles, the surface porosity as well as the overall porosity of the membranes were investigated. As shown in Fig. 3a, the surface porosity of the PSF membrane was 5.4%, while for the nanoparticle-incorporated membrane and the nanofiber-incorporated membrane were 9.7% and 16.4%, respectively. The overall porosity of PSF membrane was 28.1%, whereas the nanoparticle-incorporated membrane and the nanofiber-incorporated membrane

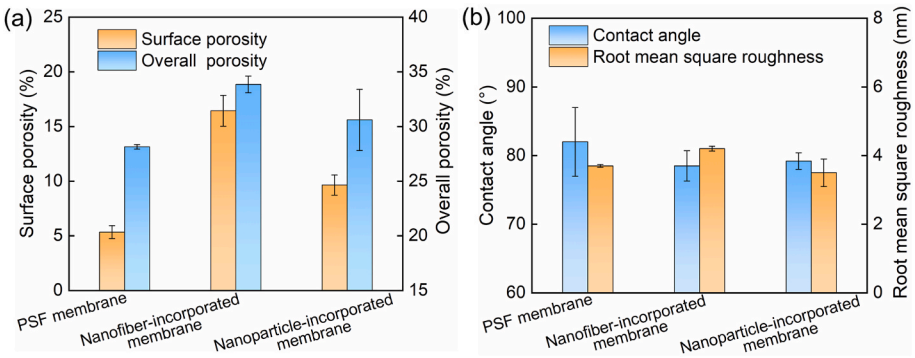

Fig. 3. Surface properties of different membranes. (a) Surface porosity and overall porosity. (b) Contact angles and root mean square roughnesses.

were 30.6% and 34.0%, respectively. Therefore, the tendency obtained here is well matched with that from the SEM analysis. In addition, the influence of TpPa nanofibers and nanoparticles on the surface properties of the membranes was investigated. The nanoparticle-incorporated membrane and the nanofiber-incorporated membrane displayed reduced water contact angles, that is, the enhanced hydrophilicities, compared with that of PSF membrane (Fig. 3b). Furthermore, these membranes did not exhibit significant difference in the aspect of the surface roughness. Thus, the enhancement of hydrophilicity can be exclusively related to the improved porosity, rather than the surface roughness. Above results, once again, proved that the incorporation of TpPa nanofibers and nanoparticles did give an influence on the porosity of the membranes.

To uncover the underlying mechanism of the porosity changes caused by the incorporation of TpPa, the phase separation behavior during the NIPS process was further studied. We first analyzed the thermodynamics of the casting solutions in terms of the cloud point and the viscosity tests, respectively. The results of cloud point tests (Fig. 4a) showed that the amount of water required to initiate the phase separation reduced from 3.6 wt% (PSF solution) to 3.2 wt% (nanofiber-incorporated PSF solution) and 3.3 wt% (nanoparticle-incorporated PSF solution), respectively. The viscosity of PSF solution was 335.7 mPa s (Fig. 4b). After the addition of TpPa, the viscosity increased to 833.0 mPa s (nanofiber-incorporated PSF solution) and 627.0 mPa s (nanoparticle-incorporated PSF solution), respectively.

Based on the aforementioned results, the mechanism of the porosity changes caused by the incorporation of TpPa can be understood (Fig. 5). Generally, the phase separation process can be divided into the instantaneous liquid-liquid demixing and the delayed liquid-liquid demixing, according to the diffusion rate of the solvent and the nonsolvent under the conditions of dynamics control [3,37,38]. The instantaneous liquid-liquid demixing process is prone to generate membranes with a loose skin layer as well as a finger-like pore structure with relatively large porosity. Whereas, a dense skin layer and a sponge-like pore structure can be easily obtained by the delayed liquid-liquid phase demixing process [39,40]. The cloud point test confirmed that the incorporation of TpPa nanoparticles and nanofibers increased the thermodynamic instability of the casting solution. In other words, the TpPa nanoparticles and nanofibers could facilitate the nonsolvent into the casting solution for the rapid exchange between nonsolvent and solvent, potentially stemming from the high porosity and relative hydrophilicity of TpPa nanofibers and nanoparticles [27]. As a result, instantaneous demixing occurred, leading to the creation of finger-like pores with larger and elongated structures [41]. This is also confirmed by the SEM analysis from the cross section of the membranes. It is worth noting that the instantaneous demixing occurred in both cases, in spite of the different surface area of TpPa nanofibers and nanoparticles.

The viscosity of the casting solution significantly increased after the incorporation of TpPa compared to that of PSF. Such increase is mainly due to the enhanced friction among polymer chains in bulk polymer solutions, originating from the incorporation of TpPa [14]. It is widely recognized that increasing the viscosity could contain the instantaneous demixing to a certain extent, thus inhibiting the growth of the finger-like pore structure [38]. However, as indicated by the cloud point test, the instantaneous demixing still occurred, in spite of the significantly increased viscosity of casting solutions. Such contradiction can be explained by a small number of TpPa being incorporated in the casting solution, which is insufficient to influence the thermodynamic state of the casting solutions. Thus, without changing the instantaneous demixing state, appropriate deceleration of the demixing by the increased viscosity ensures that the original tiny pores could merge and grow into relatively large pores [42]. This is well in line with that in SEM analysis from the surface of the membranes.

Compared with the instantaneous demixing in the nanoparticle-incorporated membrane, the nanofiber-incorporated membrane exhibited much pronounced instantaneous demixing (Fig. 5). This is largely attributed to the one-dimensional structure of TpPa nanofibers that weakens the entanglement of the surrounding PSF linear chains, compared with that of TpPa nanoparticles with small and irregular shapes. Moreover, this would generate the relatively loose structures between the nanofiber and the PSF matrices, which may account for the higher porosity appeared in the nanofiber-incorporated membrane. The improved porosity originating from the loose structures may function as additional channels, which is beneficial for the fast water permeation.

3.3. Separation performance of membranes

To elucidate the interplay of microstructures and separation performances, the ultrafiltration performances of membranes fabricated with various mass fractions of TpPa nanofibers were investigated. As shown in Fig. 6a, in the absence of TpPa nanofibers, the PSF membrane has a water permeance of 218.6 L m^{-2} h^{-1} bar^{-1} and a BSA rejection rate of 91.5%. When the addition of TpPa nanofibers was 0.05 wt%, the membrane demonstrated a slightly increased water permeance of 286.6 L m^{-2} h^{-1} bar^{-1} with a BSA rejection rate of 93.7%. When the addition of TpPa nanofibers was 0.1 wt%, the membrane exhibited a best ultrafiltration performance. The water permeance was 424.4 L m^{-2} h^{-1} bar^{-1}, while the BSA rejection rate was 94.3%. However, with the increase of the addition of TpPa nanofibers, the water permeance of membrane began to decline. The water permeance eventually decreased to 143.0 L m^{-2} h^{-1} bar^{-1}, while the BSA rejection rate remained almost constant. When the addition of TpPa nanofibers is lower than 0.15 wt%, the water permeance of the membrane is enhanced because of the increased surface and overall porosity. However, excessive addition of TpPa nanofibers may lead to poor dispersion and agglomeration of nanofibers in the matrices, resulting in increased mass transfer resistance in the membrane. These unfavorable effects resulted in the decline of water permeance, as the addition of TpPa nanofibers is higher than 0.1 wt%. In brief, the water permeance of membranes reached a maximum first and then decreased with the addition of nanofibers,

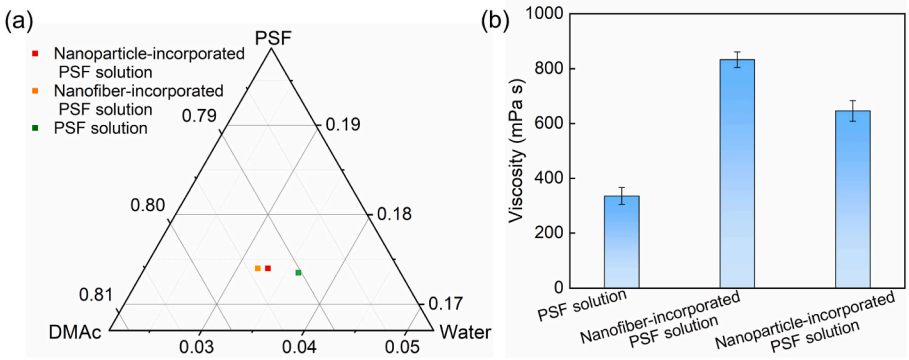

Fig. 4. (a) Ternary phase diagram and (b) viscosity of different casting solutions.

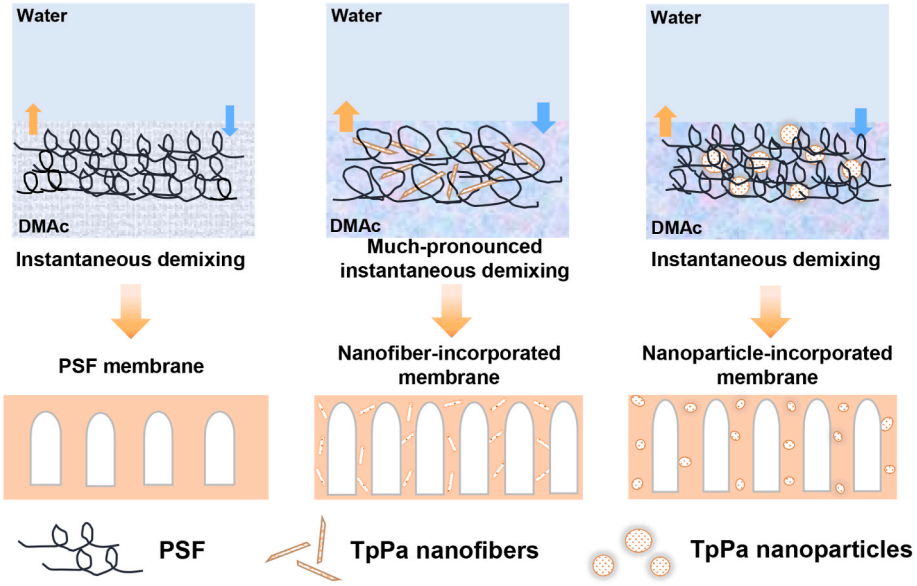

Fig. 5. Illustration of different phase separation processes.

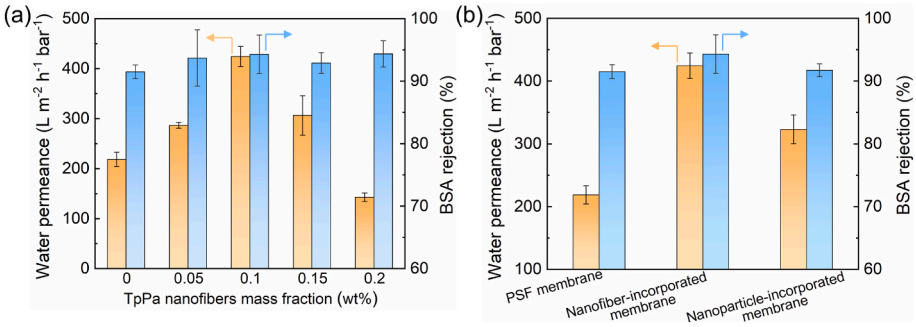

Fig. 6. (a) Effects of various mass fractions of TpPa nanofibers on water permeance and BSA rejection rate of the membranes. (b) Ultrafiltration performances of different membranes.

which is consistent with the tendency of the variation of the membrane porosity (Fig. S5). Note that the membrane thicknesses did not influence the water permeance, because they maintained unchanged regardless of the incorporation of TpPa, as we indicated above. Furthermore, the improved rejection rate of BSA may result from the improved compatibility between TpPa nanofibers and the PSF matrices, which forms well-defined membrane microstructures with less defects.

To better illustrate the influence of TpPa morphology on the membrane performance, the separation performances of the nanoparticle-incorporated membrane were tested. The water permeance of the nanoparticle-incorporated membrane was 323.2 L m^{-2} h^{-1} bar^{-1}, and the BSA rejection rate was 91.7% (Fig. 6b). Such performance was better than that of PSF membranes, as a result of the incorporation of TpPa nanoparticles. Yet, it was inferior to that of nanofiber-incorporated membrane, because of its less porous structures, as demonstrated previously. Therefore, the nanofiber-incorporated membrane demonstrated the best separation performance.

Operation stability is an important parameter for evaluating the

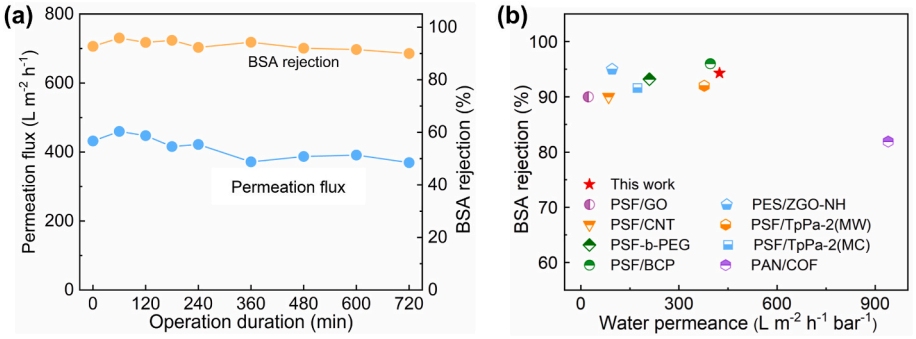

Fig. 7. (a) Changes of ultrafiltration performances of the nanofiber-incorporated membrane under a permeating duration of 720 min (The permeation flux was normalized by pressure). (b) Ultrafiltration performance comparison between our membrane with other membranes reported in literature.

membrane performance. We studied the water permeance and the BSA rejection rate of nanofiber-incorporated membrane over a period of 720 min at a pressure of 2 bar. As shown in Fig. 7a, after ultrafiltration for 720 min, the water permeance and the BSA rejection rate of the nanofiber-incorporated membrane maintained almost unchanged, compared to those of the beginning. Therefore, the nanofiber-incorporated membrane exhibited a good operation stability. In addition, the PSF membrane also displayed a good operation stability (Fig. S6). The operation stability is not compromised, in spite of the appearance of enlarged and elongated finger-liker pores. This may be attributed to the structural reinforcement of the robust TpPa nanofibers. To highlight the high water permeance in this work, the separation performance of the nanofiber-incorporated membrane is benchmarked against other state-of-the-art ultrafiltration membranes reported in literature. As shown in Fig. 7b, the nanofiber-incorporated membrane exhibited a superior performance to those of other ultrafiltration membranes (Details are listed in Table S1).

4. Conclusion

In summary, we demonstrate that the TpPa nanofibers working as the nanofillers have the advantage over the TpPa nanoparticles in the preparation of high performance MMMs. TpPa nanofibers featuring crystalline and porous structures are synthesized by a method of surfactant-mediated solvothermal synthesis. TpPa nanoparticles are also synthesized by the conventional solvothermal method. Then, they are doped into PSF to prepare MMMs via the NIPS process. It is found that the high porosity and relative hydrophilicity of TpPa nanofibers and nanoparticles lead to rapid exchange between solvent and nonsolvent, resulting in instantaneous demixing. Moreover, much pronounced instantaneous demixing occurs in the case of TpPa nanofibers being incorporated, as the one-dimensional structure weakens the entanglement of the surrounding PSF linear chains, compared with that of TpPa nanoparticles with small and irregular shapes. The nanofiber-incorporated membranes receive significantly improved porosity. The optimal nanofiber-incorporated membrane exhibits a high water permeance of up to 424.4 L m^{-2} h^{-1} bar^{-1}, together with a high rejection rate of 94.3% for BSA. This work provides a new approach for the design and fabrication of high performance MMMs using COF nanofibers as the filler. Also, it highlights the great potential of COF-nanofiber-based membrane in the application of water treatment.

Author statement

Guanghui Yang: Methodology, Investigation, Writing-Original Draft.

Zhe Zhang: Methodology, Writing-Review & Editing.

Congcong Yin: Investigation.

Xiansong Shi: Investigation.

Yong Wang: Conceptualization, Supervision, Writing-Review & Editing, Funding acquisition.

Declaration of competing interest

The authors declare that they have no known competing financial interests or personal relationships that could have appeared to influence the work reported in this paper.

Data availability

Data will be made available on request.

Acknowledgements

This work was funded by the National Natural Science Foundation of China (21825803).

Appendix A. Supplementary data

Supplementary data to this article can be found online at https://doi.org/10.1016/j.memsci.2022.120944.

References

[1] J.R. Werber, C.O. Osuji, M. Elimelech, Materials for next-generation desalination and water purification membranes, Nat. Rev. Mater. 1 (2016), 16018.
[2] N. Jacquet, S. Wurtzer, G. Darracq, Y. Wyart, L. Moulin, P. Moulin, Effect of concentration on virus removal for ultrafiltration membrane in drinking water production, J. Membr. Sci. 634 (2021), 119417.
[3] P. Li, R.L. Thankamony, X. Li, Z. Li, X. Liu, Z. Lai, Nanoporous polyethersulfone membranes prepared by mixed solvent phase separation method for protein separation, J. Membr. Sci. 635 (2021), 119507.
[4] M.R. Cervellere, X. Qian, D.M. Ford, C. Carbrello, S. Giglia, P.C. Millett, Phase-field modeling of non-solvent induced phase separation (NIPS) for PES/NMP/Water with comparison to experiments, J. Membr. Sci. 619 (2021), 118779.
[5] Y.Q. Zhang, P.L. Liu, Polysulfone (PSF) composite membrane with micro-reaction locations (MRLs) made by doping sulfated TiO_2 deposited on SiO_2 nanotubes (STSNs) for cleaning wastewater, J. Membr. Sci. 493 (2015) 275.
[6] Y. Jiang, Q. Zeng, P. Biswas, J.D. Fortner, Graphene oxides as nanofillers in polysulfone ultrafiltration membranes: shape matters, J. Membr. Sci. 581 (2019) 453–461.
[7] B. Sert, S. Gonca, Y. Ozay, E. Harputlu, S. Ozdemir, K. Ocakoglu, N. Dizge, Investigation of the antifouling properties of polyethersulfone ultrafiltration membranes by blending of boron nitride quantum dots, Colloids Surf., B 205 (2021), 111867.
[8] Z. Huang, J. Liu, Y. Liu, Y. Xu, R. Li, H. Hong, L. Shen, H. Lin, B. Liao, Enhanced permeability and antifouling performance of polyether sulfone (PES) membrane via elevating magnetic Ni@MXene nanoparticles to upper layer in phase inversion process, J. Membr. Sci. 623 (2021), 119080.
[9] L. Wu, Y. Liu, J. H, X. Feng, C. Ma, C. Wen, Preparation of polyvinylidene fluoride composite ultrafiltration membrane for micro-polluted surface water treatment, Chemosphere 284 (2021), 131294.
[10] D. Zou, Y.M. Lee, Design strategy of poly(vinylidene fluoride) membranes for water treatment, Prog. Polym. Sci. 128 (2022), 101535.
[11] J. Chen, X. Meng, Y. Tian, X. Wang, J. Zhu, H. Zheng, L. Wang, Fabrication of a superhydrophilic PVDF-*g*-PAA@FeOOH ultrafiltration membrane with visible light photo-fenton self-cleaning performance, J. Membr. Sci. 616 (2020), 118587.
[12] J. Zhao, J.Y. Chong, L. Shi, R. Wang, PTFE-assisted immobilization of pluronic F127 in PVDF hollow fiber membranes with enhanced hydrophilicity through nonsolvent-thermally induced phase separation method, J. Membr. Sci. 620 (2021), 118914.
[13] H. Sun, B. Tang, P. Wu, Development of hybrid ultrafiltration membranes with improved water separation properties using modified superhydrophilic metal-organic framework nanoparticles, ACS Appl. Mater. Interfaces 9 (2017) 21473–21484.
[14] J. Zhou, M. Yin, Z. Wang, N. Wang, Z. Qin, Q. An, Ultralow Ti_3C_2TX doping polysulfate membrane for high ultrafiltration performance, J. Membr. Sci. 637 (2021), 119603.
[15] D. Qadir, H. Mukhtar, L.K. Keong, Mixed matrix membranes for water purification applications, Separ. Purif. Rev. 46 (2016) 62–80.
[16] L. Marbelia, M.R. Bilad, I.F.J. Vankelecom, Gradual PVP leaching from PVDF/PVP blend membranes and its effects on membrane fouling in membrane bioreactors, Separ. Purif. Technol. 213 (2019) 276–282.
[17] Y. Lin, H.C. Wu, T. Yasui, T. Yoshioka, H. Matsuyama, Development of an HKUST-1 nanofiller-templated poly(ether sulfone) mixed matrix membrane for a highly efficient ultrafiltration process, ACS Appl. Mater. Interfaces 11 (2019) 18782–18796.
[18] Y. Cheng, Y. Ying, S. Japip, S.D. Jiang, T.S. Chung, S. Zhang, D. Zhao, Advanced porous materials in mixed matrix membranes, Adv. Mater. 30 (2018), 1802401.
[19] R. Liu, K.T. Tan, Y. Gong, Y. Chen, Z. Li, S. Xie, T. He, Z. Lu, H. Yang, D. Jiang, Covalent organic frameworks: an ideal platform for designing ordered materials and advanced applications, Chem. Soc. Rev. 50 (2021) 120–242.
[20] K. Geng, T. He, R. Liu, S. Dalapati, K.T. Tan, Z. Li, S. Tao, Y. Gong, Q. Jiang, D. Jiang, Covalent organic frameworks: design, synthesis, and functions, Chem. Rev. 120 (2020) 8814–8933.
[21] D.W. Sun, L.J. Huang, H.B. Pu, J. Ma, Introducing reticular chemistry into agrochemistry, Chem. Soc. Rev. 50 (2021) 1070–1110.
[22] H. Wang, H. Wang, Z. Wang, L. Tang, G. Zeng, P. Xu, M. Chen, T. Xiong, C. Zhou, X. Li, D. Huang, Y. Zhu, Z. Wang, J. Tang, Covalent organic framework photocatalysts: structures and applications, Chem. Soc. Rev. 49 (2020) 4135–4165.
[23] M.S. Lohse, T. Bein, Covalent organic frameworks: structures, synthesis, and applications, Adv. Funct. Mater. 28 (2018), 1705553.
[24] C.S. Diercks, O.M. Yaghi, The atom, the molecule, and the covalent organic framework, Science 355 (2017), eaal1585.
[25] Z. Zhang, C. Yin, G. Yang, A. Xiao, X. Shi, W. Xing, Y. Wang, Stitching nanosheets of covalent organic frameworks to build aligned nanopores in nanofiltration membranes for precise ion separations, J. Membr. Sci. 618 (2021), 118754.
[26] S. Kandambeth, A. Mallick, B.V. Lukose, M. Mane, T. Heine, R. Banerjee, Construction of crystalline 2D covalent organic frameworks with remarkable chemical (acid/base) stability via a combined reversible and irreversible route, J. Am. Chem. Soc. 134 (2012) 19524–19527.

[27] L. Xu, J. Xu, B. Shan, X.l. Wang, C.J. Gao, TpPa-2-incorporated mixed matrix membranes for efficient water purification, J. Membr. Sci. 526 (2017) 355–366.
[28] P.H.H. Duong, V.A. Kuehl, B. Mastorovich, J.O. Hoberg, B.A. Parkinson, K.D. Li-Oakey, Carboxyl-functionalized covalent organic framework as a two-dimensional nanofiller for mixed-matrix ultrafiltration membranes, J. Membr. Sci. 574 (2019) 338–348.
[29] X.Y. Wang, X.S. Shi, Y. Wang, In situ growth of cationic covalent organic frameworks (COFs) for mixed matrix membranes with enhanced performances, Langmuir 36 (2020) 10970–10978.
[30] G. Yang, Z. Zhang, C. Yin, X. Shi, Y. Wang, Polyamide membranes enabled by covalent organic framework nanofibers for efficient reverse osmosis, J. Polym. Sci. (2021), https://doi.org/10.1002/pol.20210664.
[31] G. Yang, Z. Zhang, C. Yin, X. Shi, Y. Wang, Morphology engineering for covalent organic frameworks (COFs) by surfactant mediation and acid adjustment, Chin. J. Polym. Sci. 40 (2022) 338–344.
[32] W. Sun, T. Chen, C. Chen, J. Li, A study on membrane morphology by digital image processing, J. Membr. Sci. 305 (2007) 93–102.
[33] L. Zhao, C. Wu, Z. Liu, Q. Zhang, X. Lu, Highly porous PVDF hollow fiber membranes for VMD application by applying a simultaneous co-extrusion spinning process, J. Membr. Sci. 505 (2016) 82–91.
[34] C.H. Loh, R. Wang, L. Shi, A.G. Fane, Fabrication of high performance polyethersulfone UF hollow fiber membranes using amphiphilic Pluronic block copolymers as pore-forming additives, J. Membr. Sci. 380 (2011) 114–123.
[35] S. Liu, Y. Chu, C. Tang, S. He, C. Wu, High-performance chlorinated polyvinyl chloride ultrafiltration membranes prepared by compound additives regulated non-solvent induced phase separation, J. Membr. Sci. 612 (2020), 118434.
[36] R. Wang, X. Shi, Z. Zhang, A. Xiao, S. Sun, Z. Cui, Y. Wang, Unidirectional diffusion synthesis of covalent organic frameworks (COFs) on polymeric substrates for dye separation, J. Membr. Sci. 586 (2019) 274–280.
[37] R.M. Boom, I.M. Wlenk, T. Boomgaard, C.A. Smolders, Microstructures in phase inversion membranes. part 2. the role of a polymeric additive, J. Membr. Sci. 73 (1992) 277–292.
[38] G.R. Guillen, Y. Pan, M. Li, E.M.V. Hoek, Preparation and characterization of membranes formed by nonsolvent induced phase separation: a review, Ind. Eng. Chem. Res. 50 (2011) 3798–3817.
[39] F. Lessan, R. Foudazi, Effect of [EMIM][BF_4] ionic liquid on the properties of ultrafiltration membranes, Polymer 210 (2020), 122977.
[40] I.H. Alsohaimi, M. Kumar, M.S. Algamdi, M.A. Khan, K. Nolan, J. Lawler, Antifouling hybrid ultrafiltration membranes with high selectivity fabricated from polysulfone and sulfonic acid functionalized TiO_2 nanotubes, Chem. Eng. J. 316 (2017) 573–583.
[41] C. Kahrs, J. Schwellenbach, Membrane formation via non-solvent induced phase separation using sustainable solvents: a comparative study, Polymer 186 (2020), 122071.
[42] E.D. Siggia, Late stages of spinodal decomposition in binary mixtures, Phys. Rev. A 20 (1979) 595–605.